
This is an electronic reprint of the original article.
This reprint may differ from the original in pagination and typographic detail.

Laakso, Sampsa V.A.; Johansson, Jakob; Johansson, Daniel; Schultheiss, Fredrik; Ståhl, Jan Eric

Multi-objective testing of different brass alloy components for DFM

Published in:
Procedia CIRP

DOI:
[10.1016/j.procir.2019.03.023](https://doi.org/10.1016/j.procir.2019.03.023)

Published: 01/01/2019

Document Version
Publisher's PDF, also known as Version of record

Please cite the original version:
Laakso, S. V. A., Johansson, J., Johansson, D., Schultheiss, F., & Ståhl, J. E. (2019). Multi-objective testing of different brass alloy components for DFM. *Procedia CIRP*, 81, 127-132.
<https://doi.org/10.1016/j.procir.2019.03.023>

This material is protected by copyright and other intellectual property rights, and duplication or sale of all or part of any of the repository collections is not permitted, except that material may be duplicated by you for your research use or educational purposes in electronic or print form. You must obtain permission for any other use. Electronic or print copies may not be offered, whether for sale or otherwise to anyone who is not an authorised user.

52nd CIRP Conference on Manufacturing Systems

Multi-objective testing of different brass alloy components for DFM

Sampsa V.A. Laakso^{*a}, Jakob Johansson^b, Daniel Johansson^b, Fredrik Schultheiss^b, Jan-Eric Ståhl^b

^a Aalto University School of Engineering, Puumiehenkuja 3, Espoo, 02150, Finland

^b Lund University, Production and Materials Engineering, Ole Römers Väg 1, Lund, 223 63, Sweden

* Corresponding author. Tel.: +358407055039; E-mail address: sampsa.laakso@aalto.fi

Abstract

This paper investigates the differences of leaded and low-lead brasses in terms of mechanical and thermal properties, machinability and product strength using physical testing and simulations. The information can be used in companies for Design for Manufacturability (DFM) while designing processes for lead free brass. The novelty of this research is to combine data from different testing methods to a unified model that can be used in both cutting simulations and product simulations.

© 2019 The Authors. Published by Elsevier Ltd.

This is an open access article under the CC BY-NC-ND license (<http://creativecommons.org/licenses/by-nc-nd/3.0/>)

Peer-review under responsibility of the scientific committee of the 52nd CIRP Conference on Manufacturing Systems.

Keywords: Metal Cutting; Multi-objective testing; FEM

1. Introduction

Traditional free machining brass is known to release lead in contact with water, which has caused many countries to restrict the lead content for alloys and products in contact with tap water.[1] Rules and regulation in combination with market demand and requirement for more sustainable production has changed the brass industry significantly into using materials with lower lead content. Design and manufacturing of products in low-lead brass (< 0.2 wt. %) presents numerous technical challenges for the industry in comparison to traditional free machining brass with 3 - 4 wt. % of lead. The machinability of low-lead brass is generally lower compared to leaded brass but also mechanically stronger which can allow for more thin-walled products and thus, balances the manufacturing cost through decreased material consumption.[2] In order to analyze the cost effects quantitatively with modern digital manufacturing tools, i.e. simulations, the material needs to be modelled. This paper shows how different experimental methods can be used for multiple purposes. The multi-objective testing includes tensile

testing, torsion testing, cutting experiments and thermal testing.

Nomenclature

A	Johnson-Cook yield stress equivalent
a_p	cutting depth
B	Johnson-Cook strain hardening coefficient
C	Johnson-Cook rate hardening coefficient
C_{crit}	Cockcroft-Latham critical damage value
$\dot{\epsilon}_{ref}$	reference strain rate
m	Johnson-Cook thermal softening exponent
n	Johnson-Cook strain hardening exponent
T_{melt}	melting temperature
T_{ref}	reference temperature
v_C	cutting speed
f	cutting feed

Each of the testing methods contribute to the individual objective but also to the material model, that can be used for simulations of different design and manufacturing stages. For

example, the torsion testing produces data about the mechanical properties of the product but also the damage behavior can be measured from the torsion tests for cutting simulations. Machinability issues of low-lead brass have been investigated in [3–5]. The outcome is that high cutting speed and relatively small feed improves the chip breakage while machining low-lead brass. Similar studies have been made by Laakso & Niemi in 2016 [4] and Schultheiss et al. 2017 [5]. The latter investigates six different brass alloys, one with high lead content and other without or with very low lead. The outcome is that machinability of low-lead brass is poor in comparison to CW614N and especially chip formation leads to long chips and poor chip breakage. Tool wear rate and cutting forces are higher with low-lead brass [8]. CW724R is an exception from this and the chip formation is manageable but tool wear and cutting resistance are higher than in reference group, which is concluded also in Schultheiss et al. where comparison is done between CW724R and CW614N. One approach to overcome the issues of lead is to replace it with bismuth. Atsumi et al. 2011 have investigated the machinability and mechanical properties of such a brass, and showed that even though machinability was 75 % of the machinability of leaded brass, the mechanical properties of bismuth brass were superior [8]. Some consider using bismuth instead of lead shortsighted since bismuth is toxic as well [9] and even though bismuth has poor solubility to water, it has caused issues with aquatic birds ingesting bismuth shotshells [10].

FEM modelling of metal cutting has been an active research field for a few decades and much advances have been done in the field regarding material model accuracy, modelling the contact between tool and chip among other aspects of the models [7–9]. There has not been a paper where the same model has been used for both metal cutting simulations and simulating the product strength. In addition to presenting the multi-objective use of the testing methods, this paper also shows the results of the same model in product simulations and cutting simulations.

This paper shows that the same model can be used for product simulations and process simulations when the material properties are acquired from different testing methods. The methods in this work are tensile testing, LFA thermal testing, torsion testing and cutting experiments. Tensile testing provides the basis of the mechanical behavior of the materials. LFA testing is used for acquiring temperature dependent thermal properties, which are shown to be important regarding FEM modelling accuracy in Laakso 2017 [7]. Cutting experiments and torsion testing of the final component are used for evaluating machinability and product strength, but also for verifying the simulation results and acquiring damage or fracture behavior of the materials. The concept of using cutting experiments for determining material properties and fracture behavior is discussed in depth in [8–10].

2. Materials and methods

The brass alloys used in this research are CW614N, a typical leaded, free machining brass and CW724R, a silicon alloyed brass with high copper- and very low lead content.

The composition of the materials is shown in table 1. The component is a three-way coupling (brass part shown in Fig. 1) that has to withstand enough pressure during operation and torsional stress during installation. Two different geometries of the components are tested, one for each brass alloy.

Table 1. Material composition as in EN12167 standard.

(wt. %)	Cu	Pb	Si	P	Zn
CW614N	57-59	2.5-3.5	-	-	Rest
CW724R	75-77	Max 0.09	2.7-3	0.02-0.1	Rest

Wall thickness for CW724R is approximately 87% of the wall thickness of the component for CW614N. The component is forged at 700 °C and machined to a final shape. Tensile testing was done according to ISO 6892-1 for the brass billets in as-delivered state, using standard tensile testing setup. Each test was repeated three times. Thermal testing was done with LFA (Light Flash Apparatus) method, using NETZSCH Hyper Flash LFA 467 HT equipment. Torsion testing was done with specially manufactured equipment. The setup consists of electrical motor, reduction drive, component fixtures, and Kistler quartz torque dynamometer type 9275, that are shown in Fig. 1. The torsion has a rotational speed of 0.588 deg/s.

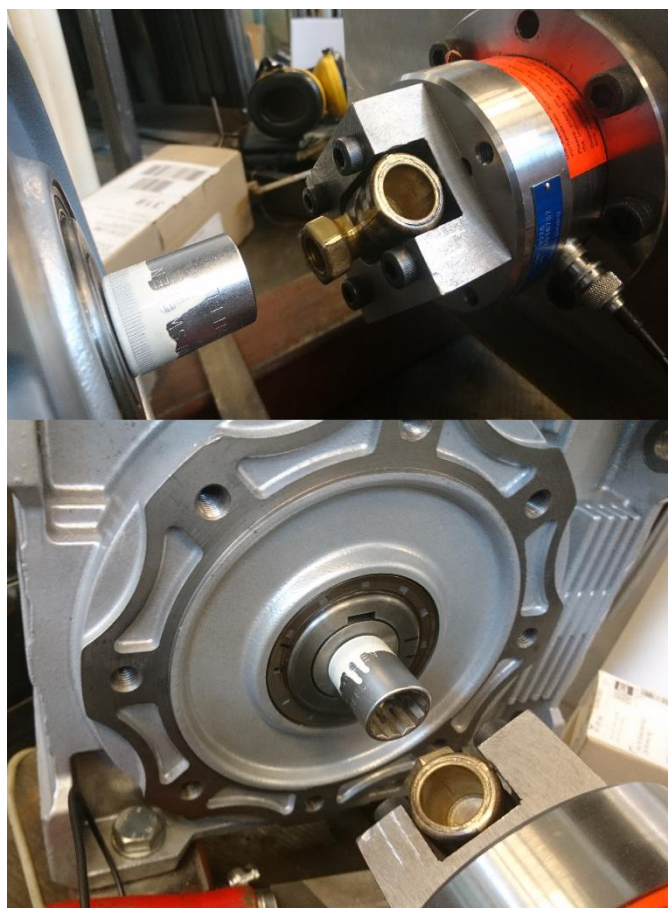


Fig. 1. Torsion testing equipment.

2.1. Cutting Experiments

Cutting experiments were done with a SMT 500 Swedturn NC-lathe. The cutting parameters were: $v_c = 400$ mm/min,

$a_p = 0.5, 1, 1.5, 2, 2.5$ mm, $f = 0.05, 0.1, 0.15, 0.2, 0.25$ and 0.3 mm/rev. The cutting inserts were plane grinded to 0° rake angle from DNGA150708F. Insert material was H10F cemented carbide.

2.2. Simulations

Simulations were done with SFTC Deform FEM software. Torsion simulations are in 3D and cutting simulations in 2D. The 3D torsion simulations have ~ 200000 elements in an elasto-plastic workpiece. The fixturing was modelled as rigid. The model setup is shown in Fig. 2. Johnson-Cook material model (Eq. 1) was fitted to tensile testing data for both materials. Cockcroft-Latham damage model (Eq. 2) was used for fracture initiation and damage evolution. The damage model was fitted to the fracture strains of the materials, and adjusted further using the torsion testing and cutting experiments for reference. The material model parameters are given in table 2 that are acquired by fitting the model to the data presented in Fig. 4. The parameter A value for CW724R in annealed state was selected to fit material suppliers (Wieland) value for yield stress in annealed state.¹

$$\sigma = (A + B\varepsilon^n) \left[1 + C \ln\left(\frac{\dot{\varepsilon}}{\dot{\varepsilon}_{ref}}\right) \right] \left[1 - \left(\frac{T - T_{ref}}{T_{melt} - T_{ref}}\right)^m \right] \quad (1)$$

$$C_{crit} = \int^\varepsilon \sigma^* d\varepsilon \quad (2)$$

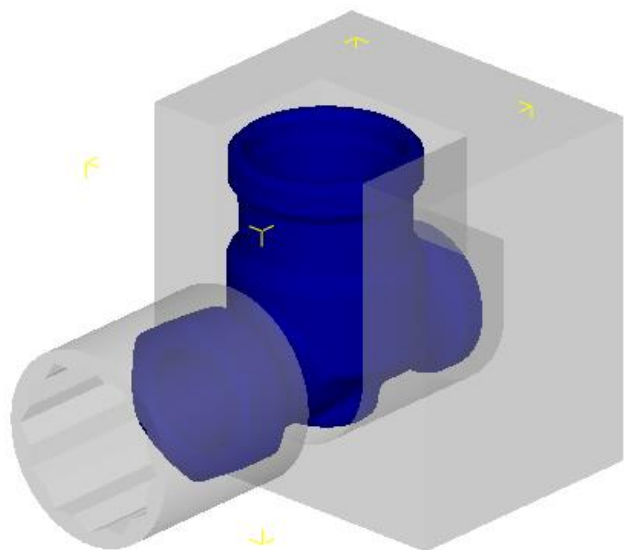


Fig. 2. The torsion simulation setup, workpiece in blue, fixturing in gray.

Cutting simulations were done with an elasto-plastic workpiece and a rigid tool. The workpiece was meshed with 3500 elements and the mesh was refined so that 15 elements were in the cutting depth, as shown in Fig. 3. The time step was $0.75 \mu s$ and the simulations had 1000 steps. Cutting

parameters were the same as in cutting experiments. The same material model was used as in torsion simulations. Shear friction of 0.5 was used in tool-chip contact.

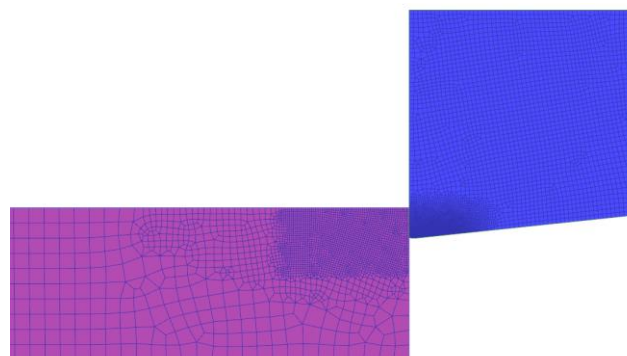


Fig. 3. Cutting simulation setup.

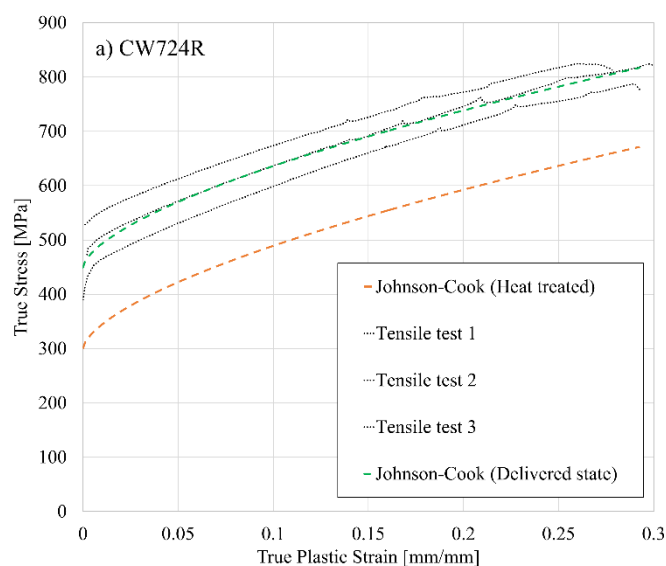
Table 2. Material model parameters.

	CW614N	CW724R annealed	CW724R as delivered
A	231	300	449
B	770	804	798
C	0.0935	0.001	0.001
n	0.589	0.628	0.6316
m	1.0	1.0	1.0
T_{ref}	20	20	20
T_{melt}	885	900	900
$\dot{\varepsilon}_{ref}$	0.001	0.001	0.001
C_{crit}	117	80	80

3. Results

3.1. Tensile testing

Tensile testing results are shown in Fig. 4, with corresponding Johnson-Cook model curves. For CW724R the standard deviation between the three tests was relatively high, being approximately 5 %. For CW614N the standard deviation was 2.3 %.



¹ https://www.wieland.com/files/pdfs/download_pdfs_en/products_ex/ECOB_RASS-Thelead-freemachiningbrass.pdf, referred on 6.3.2019

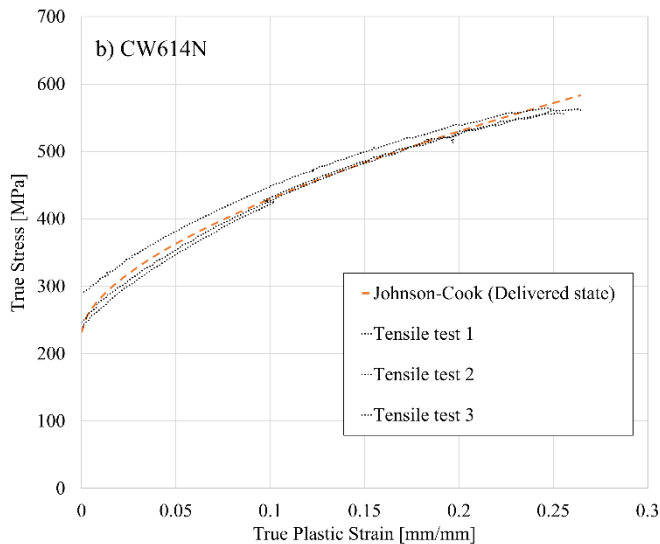


Fig. 4. Tensile testing results and corresponding Johnson-Cook models for a) CW724R and b) CW614N.

3.2. Thermal testing

Table 3 presents the thermal testing results for the materials in four different temperatures. The tested values are heat capacity and thermal conductivity.

Table 3. LFA testing results for heat capacity and thermal conductivity.

T [°C]	CW614N		CW724R	
	C_p [J/g*K]	k [W/m*K]	C_p [J/g*K]	k [W/m*K]
20	0.363	105.223	0.383	32.407
100	0.367	113.061	0.388	37.859
200	0.382	124.729	0.404	45.392
300	0.433	140.111	0.48	59.666

3.3. Torsion testing and simulations

Torsion testing results in Fig. 5 show unexpectedly large variation regarding CW724R with maximum fracture load being 180 Nm and minimum 92 Nm. CW614N has more consistent behavior with maximum load of 151 Nm and minimum 142 Nm. The simulation overestimated the results for CW724R since the fracture load was 150 Nm in as delivered state. Simulation accuracy was satisfactory in annealed state of CW724R with fracture load of 122 Nm. Regarding the CW614N, the simulation grossly overestimated the fracture load and resulted in 210 Nm. Fig. 6 presents the simulation output and illustrates the location of the fracture.

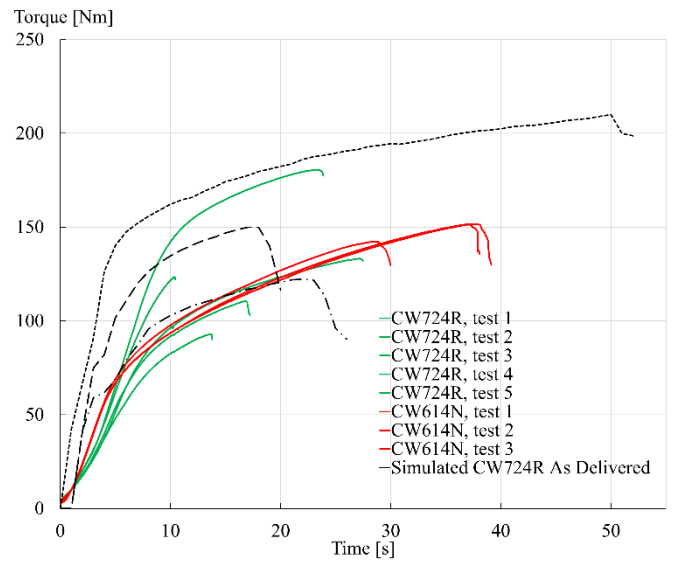


Fig. 5. Torsion testing and simulation results.

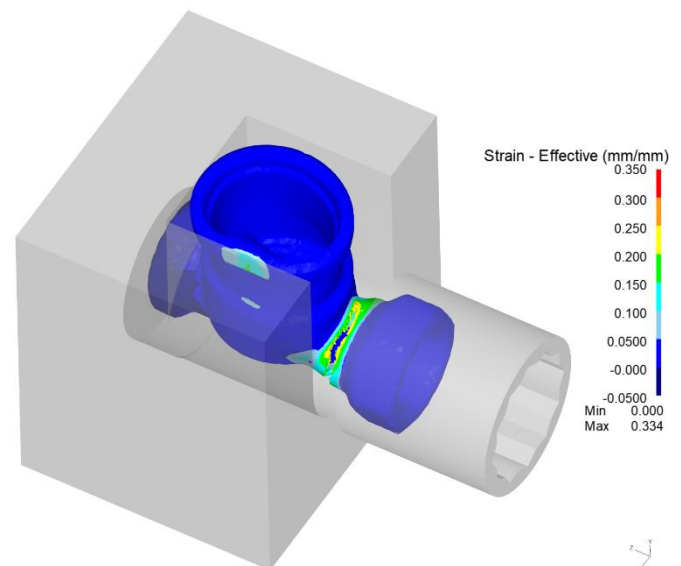


Fig. 6. Torsion simulation output for CW724R.

3.4. Cutting Experiments and simulations

Cutting experiments and simulations are evaluated with cutting forces and feed forces. The simulation output is shown in Fig. 7 and the forces are presented in Table 4. The chip serration frequency changes significantly between the annealed and as-delivered state of CW724R. The average simulation error for annealed CW724R model is 27 % for cutting force and 47 % for feed force. Model of CW724R in as-delivered state produced 14 % and 39 % errors correspondingly. The model for CW614N produced 18 % and 30 % errors for cutting force and feed force respectively.

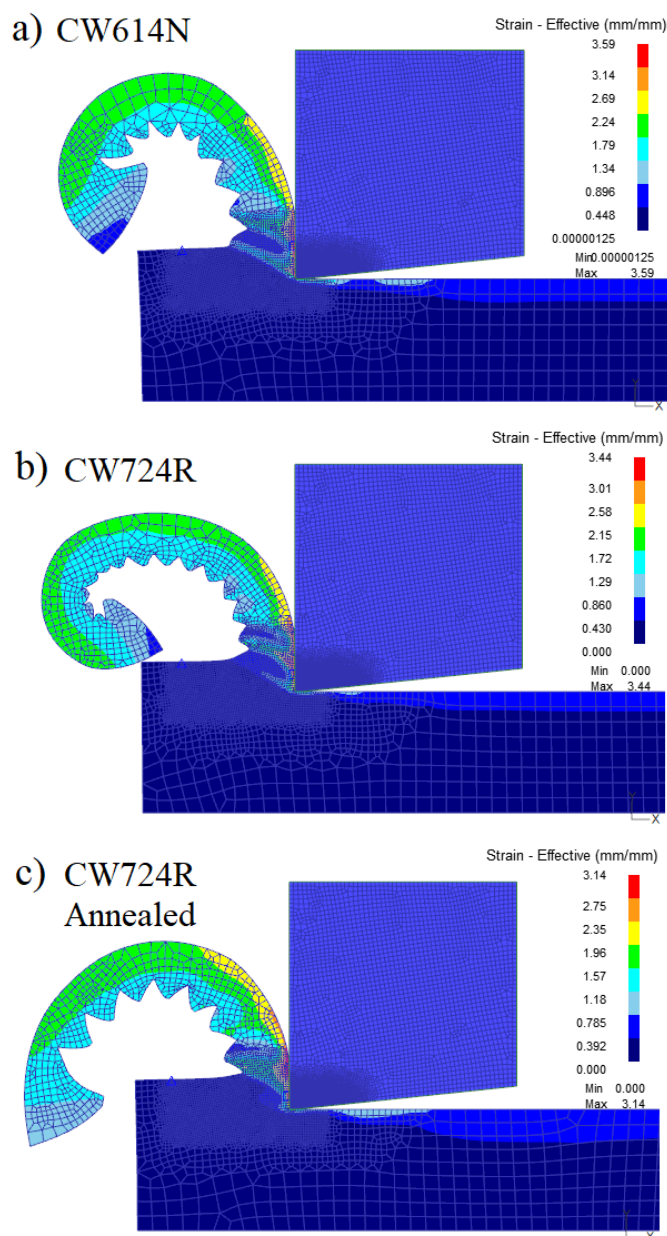


Fig. 7. Output of the cutting simulations for 0.2 mm/rev feed. a) CW614N, b) CW724R in as delivered state and c) CW724R in annealed state.

Table 4. Cutting forces from experiments and simulations with corresponding errors.

CW724R		Experiment					Simulation in as delivered state				
feed [mm/rev]		F_c [N]	F_f [N]	F_c [N]	Error	F_f [N]	Error	F_c [N]	Error	F_f [N]	Error
0.1		142	72	106	-26 %	44	-39 %				
0.2		234	98	230	-2 %	54	-45 %				
0.3		317	121	362	14 %	82	-32 %				
avg. Error				14 %		39 %					
CW724R		Experiment					Simulation in annealed state				
feed [mm/rev]		F_c [N]	F_f [N]	F_c [N]	Error	F_f [N]	Error	F_c [N]	Error	F_f [N]	Error
0.1		142	72	86	-39 %	37	-48 %				
0.2		234	98	176	-25 %	48	-51 %				
0.3		317	121	266	-16 %	70	-42 %				
avg. Error				27 %		47 %					
CW614N		Experiment					Simulation in as delivered state				
feed [mm/rev]		F_c [N]	F_f [N]	F_c [N]	Error	F_f [N]	Error	F_c [N]	Error	F_f [N]	Error
0.1		104	47	85	-18 %	33	-29 %				
0.2		168	70	190	13 %	46	-35 %				
0.3		232	91	287	24 %	67	-27 %				
avg. Error				18 %		30 %					

4. Discussion and conclusions

This paper shows how different testing methods can be used to build unified model that can be used for component strength simulations as well as for simulating manufacturing processes. The testing methods were tensile testing, torsion testing, thermal testing and cutting experiments. Tensile testing provided the foundation for the mechanical behavior. Torsion testing was done to verify the strength of the final product and to calibrate the fracture model. Thermal testing was done to include temperature dependent thermal properties, i.e. heat capacity and conductivity to the simulation models. Cutting experiments were done to test the machinability of the materials but also to calibrate the FEM model.

The combination of torsion testing and cutting experiments proved to be a critical step to identify the behavior of the materials. If either one was used alone, the simulation models would have been calibrated to fit the performed experiments, but the simulation results would have not been correct for the missing experiments. Since the both of the experiments were done, the error identified a missing factor in the simulation model. The material was annealed during the forging and it would have been overlooked if the simulations and experiment did not reveal the error. Since the cutting experiments and tensile testing were done in as-delivered state, the material properties identified from these did not represent the material properties of the final product that was in fact annealed in the process of forging. This can be identified from the results by looking at the torsion simulation error of CW614N in as-delivered state, which is unreasonably high. The same can be seen in the cutting simulation error for the annealed state of CW724R that is higher than the

corresponding error in as-delivered state. Other sources of error regarding the torsion simulations are the inaccuracies of the CAD model used in the simulations. The physical forged products were measured to have deviation from the intended geometry. Cutting simulations have additional errors from the simplified tool geometry and friction model.

The presented case study of the three-way couplings and the machining of two different brass alloys revealed the following conclusions:

1. The same model can be used for simulating both component strength and cutting process with reasonable accuracy.
2. Even a small difference in component geometry compared to the CAD-model has significant effect on the simulation accuracy.
3. Microstructural effects must be taken into account either by simulations or by testing the material in operation conditions. In this case, the annealing effect of forging at 700 degrees had clear effect on material properties. The cutting simulations done with annealed material properties did not fit the cutting experiments done with CW724R in as delivered state and the torsion simulation done with material properties in as delivered state didn't fit the experiment done in annealed state.

In order to improve the modelling accuracy, material properties need to be tested in both as delivered state and in annealed state. The possible effect of residual strains after forging should be considered. Residual strains can be evaluated by measuring the microstructure and strains from forged workpiece and with microstructural simulations of the workpiece in forging process. For future work, the workpiece geometry needs to be 3D scanned in order to eliminate the geometrical error and compare the deformed and fractured product with the simulated geometry after failure.

References

- [1] Tong, S., von Schirmding, Y. E., Prapamontol, T., 2000, Environmental lead exposure: a public health problem of global dimensions., *Bulletin of the World Health Organization*, 78/9:1068–1077.
- [2] Vilarinho, C., Davim, J. P., Soares, D., Castro, F., Barbosa, J., 2005, Influence of the chemical composition on the machinability of brasses, *Journal of Materials Processing Technology*, 170/1:441–447, DOI:https://doi.org/10.1016/j.jmatprotec.2005.05.035.
- [3] Laakso, S. V. A., Hokka, M., Niemi, E., Kuokkala, V.-T., 2013, Investigation of the effect of different cutting parameters on chip formation of low-lead brass with experiments and simulations, *Proceedings of the Institution of Mechanical Engineers, Part B: Journal of Engineering Manufacture*, 227/11, DOI:10.1177/0954405413492732.
- [4] Laakso, S. V. A., Niemi, E., 2016, Modified Johnson-Cook flow stress model with thermal softening damping for finite element modeling of cutting, *Proceedings of the Institution of Mechanical Engineers, Part B: Journal of Engineering Manufacture*, 230/2, DOI:10.1177/0954405415619873.
- [5] Gane, N., 1981, The effect of lead on the friction and machining of brass, *Philosophical Magazine A*, 43/3:545–566, DOI:10.1080/01418618108240394.
- [6] Schultheiss, F., Johansson, D., Bushlya, V., Zhou, J., Nilsson, K., et al., 2017, Comparative study on the machinability of lead-free brass, *Journal of Cleaner Production*, 149:366–377, DOI:https://doi.org/10.1016/j.jclepro.2017.02.098.
- [7] Nobel, C., Klocke, F., Lung, D., Wolf, S., 2014, Machinability Enhancement of Lead-free Brass Alloys, *Procedia CIRP*, 14:95–100, DOI:https://doi.org/10.1016/j.procir.2014.03.018.
- [8] Bushlya, V., Johansson, D., Lenrick, F., Ståhl, J.-E., Schultheiss, F., 2017, Wear mechanisms of uncoated and coated cemented carbide tools in machining lead-free silicon brass, *Wear*, 376–377:143–151, DOI:https://doi.org/10.1016/j.wear.2017.01.039.
- [9] Atsumi, H., Imai, H., Li, S., Kondoh, K., Kousaka, Y., et al., 2011, High-strength, lead-free machinable α - β duplex phase brass Cu–40Zn–Cr–Fe–Sn–Bi alloys, *Materials Science & Engineering A*, 529/Complete:275–281, DOI:10.1016/j.msea.2011.09.029.
- [10] Gad, S. C., 2014, *Bismuth*, P. B. T.-E. of T. (Third E. Wexler, Ed. Oxford: Academic Press, pp. 512–513.
- [11] Fahey, N. S. C., 2005, THE USE OF SCIENCE IN ENVIRONMENTAL POLICY MAKING AND THE IMPLICATIONS FOR HEALTH: A CASE STUDY OF BISMUTH SHOTSHELLS. UWSpace.
- [12] Arrazola, P. J., Özel, T., Umbrello, D., Davies, M., Jawahir, I. S., 2013, Recent advances in modelling of metal machining processes, *CIRP Annals - Manufacturing Technology*, 62/2:695–718, DOI:http://dx.doi.org/10.1016/j.cirp.2013.05.006.
- [13] Mackerle, J., 1999, Finite-element analysis and simulation of machining: a bibliography (1976–1996), *Journal of Materials Processing Technology*, 86/1–3:17–44, DOI:http://dx.doi.org/10.1016/S0924-0136(98)00227-1.
- [14] Mackerle, J., 2003, Finite element analysis and simulation of machining: an addendum: A bibliography (1996–2002), *International Journal of Machine Tools and Manufacture*, 43/1:103–114, DOI:http://dx.doi.org/10.1016/S0890-6955(02)00162-1.
- [15] Laakso, S. V. A., 2017, Heat matters when matter heats – The effect of temperature-dependent material properties on metal cutting simulations, *Journal of Manufacturing Processes*, 27:261–275, DOI:10.1016/j.jmapro.2017.03.016.
- [16] Laakso, S. V. A., Niemi, E., 2016, Determination of material model parameters from orthogonal cutting experiments, *Proceedings of the Institution of Mechanical Engineers, Part B: Journal of Engineering Manufacture*, 230/5, DOI:10.1177/0954405414560620.
- [17] Agmell, M., Ahadi, A., Ståhl, J.-E., 2013, The Link Between Plasticity Parameters and Process Parameters in Orthogonal Cutting, *Procedia CIRP*, 8:224–229, DOI:http://dx.doi.org/10.1016/j.procir.2013.06.093.
- [18] Laakso, S. V. A., Väänänen, A., Bossuyt, S., Arkkio, A., 2018, Dull punch line is not a joke – Worn cutting edge causes higher iron losses in electrical steel piercing, *Robotics and Computer-Integrated Manufacturing*, DOI:10.1016/j.rcim.2018.03.006.